

Heavy dense QCD from a 3d effective lattice theory

Jonas Glesaaen*, Mathias Neuman, Owe Philipsen*

Institut für Theoretische Physik - Johann Wolfgang Goethe-Universität

Max-von-Laue-Str. 1, 60438 Frankfurt am Main, Germany

E-mail: glesaaen, philipsen@th.physik.uni-frankfurt.de

The cold and dense regime of the QCD phase diagram is to this day inaccessible to first principle lattice calculations owing to the sign problem. Here we present progress of an ongoing effort to probe this particularly difficult regime utilising a dimensionally reduced effective lattice theory with a significantly reduced sign problem. The effective theory is derived by combined character and hopping expansion and is valid for heavy quarks near the continuum. We show an extension of the effective theory to order $u^5 \kappa^8$ in the cold regime. A linked cluster expansion is applied to the effective theory resulting in a consistent mechanism for handling the effective theory fully analytically. The new results are consistent with the ones from simulations confirming the viability of analytic methods. Finally we resum the analytical result which doubles the convergence region of the expansion.

The 33rd International Symposium on Lattice Field Theory

14 -18 July 2015

Kobe International Conference Center, Kobe, Japan

*Speakers.

1. Introduction

The details of the QCD phase diagram are still largely unknown because of the sign problem of Monte Carlo simulations of lattice QCD. Approximate methods are able to circumvent this problem only for small quark chemical potentials $\mu = \mu_B/3 \lesssim T$ [1]. So far, no sign of a critical point or a first order phase transition has been found in this controlled region. Complex Langevin algorithms do not suffer from the sign problem, but in some models converge to incorrect answers or in QCD are restricted to certain regions in parameter space. A lot of progress has been made recently, but no true phase transition has been reported in this approach either [2].

These difficulties have motivated the development of effective lattice theories, which can either be handled analytically or whose sign problem is mild enough to simulate the cold and dense region of QCD. Here we update an ongoing project to describe the cold and dense regime of QCD by means of a 3d effective theory, which is derived by combined strong coupling and hopping expansions. The resulting effective theory is valid for the description of very heavy quarks for sufficiently weak couplings, such that a continuum limit of thermodynamic functions can be attempted. Its sign problem is mild enough for complex Langevin or even Monte Carlo simulations to describe cold nuclear matter. The heavy dense region is also studied by complex Langevin simulations in 4d [3], for which the effective theory results can serve as a benchmark. Furthermore, the effective theory approach can be tested against full simulations in two-colour QCD [4, 5]. In a new development, we show how the thermodynamic functions of the effective theory can also be computed fully analytically by means of linked cluster expansion.

2. Derivation of the effective theory

We start on a $(3+1)$ -dimensional lattice with Wilson's gauge and fermion actions on infinite spatial volume and at finite temperature $T = (aN_\tau)^{-1}$. After Grassmann integration the partition function is

$$Z = \int [dU_\mu] \det [Q]^{N_f} \exp [S_g] , \quad S_g = \frac{\beta}{2N_c} \sum_p [\text{tr } U_p + \text{tr } U_p^\dagger] , \quad (2.1)$$

with the quark hopping matrix

$$Q_{\alpha\beta,xy}^{ab} = \delta^{ab} \delta_{\alpha\beta} \delta_{xy} - \kappa \sum_{\hat{v}=0}^3 \left[e^{a\mu\delta_{v0}} (1 + \gamma_v)_{\alpha\beta} U_v^{ab}(x) \delta_{x,y-\hat{v}} + e^{-a\mu\delta_{v0}} (1 - \gamma_v)_{\alpha\beta} U_{-v}^{ab}(x) \delta_{x,y+\hat{v}} \right] .$$

The lattice gauge coupling and hopping parameter are defined as

$$\beta = \frac{2N_c}{g^2}, \quad \kappa = \frac{1}{2am + 8} . \quad (2.2)$$

A 3d effective action is then defined by integrating out the spatial link variables

$$Z = \int [dU_0] e^{-S_{\text{eff}}[U_0]} = \int [dW] e^{-S_{\text{eff}}[W]}, \quad e^{S_{\text{eff}}} \equiv \int [dU_k] \det [Q]^{N_f} \exp [S_g] . \quad (2.3)$$

The resulting effective theory depends on temporal link variables closing through the temporal boundary, i.e. on Polyakov loops

$$W_i \equiv \prod_{\tau=1}^{N_\tau} U_0(\vec{x}_i; \tau), \quad L_i = \text{tr} W_i. \quad (2.4)$$

Without truncations, the effective action is unique and exact. Since all spatial links are integrated over, the resulting effective action has long-range interactions of Polyakov loops at all distances and to all powers so that in practice truncations are necessary. For non-perturbative ways to determine truncated theories, see [6, 7, 8, 9]. Here we expand eq. (2.3) in a combined strong coupling and hopping expansion, with interaction terms ordered according to their leading powers in β, κ .

For the gauge action it is advantageous to perform a character expansion

$$\exp \left[\frac{\beta}{2N_c} \left(\text{tr} U + \text{tr} U^\dagger \right) \right] = c_0(\beta) \left[1 + \sum_{r \neq 0} d_r a_r(\beta) \chi_r(U) \right], \quad (2.5)$$

where the factor $c_0(\beta)$ can be neglected as it is independent of gauge links and cancels in expectation values. In earlier publications [10, 11], we have shown how to compute the effective gauge theory up to rather high orders in the fundamental character expansion coefficient $u(\beta) \equiv a_f(\beta)$. Note that $u(\beta) = \beta/18 + O(\beta^2) < 1$, thus improving the convergence compared to straightforward expansion in β . To leading order the effective gauge action reads

$$e^{S_{\text{eff}}^{(1)}} = \lambda(u, N_\tau) \sum_{\langle ij \rangle} (L_i L_j^* + L_i^* L_j), \quad \lambda(u, N_\tau) = u^{N_\tau} [1 + \dots], \quad (2.6)$$

where higher order corrections of $\lambda(u, N_\tau)$ as well as a discussion of higher order interaction terms can be found in [10]. Going via an effective action results in a resummation with better convergence properties than a direct series expansion of the thermodynamic observables as in [12, 13]. We observe that $\lambda(u, N_\tau)$ is suppressed for large N_τ . In this presentation our main interest is in the cold and dense region, for which all $\lambda_i < 10^{-18}$ and the pure gauge contribution can be safely neglected.

To compute the quark determinant in a spatial hopping expansion, we split the quark matrix in positive and negative temporal and spatial parts,

$$Q = 1 - T - S = 1 - T^+ - T^- - S^+ - S^-, \quad (2.7)$$

The static determinant is given by neglecting the spatial parts and can be computed exactly [14]

$$\begin{aligned} \det[Q_{\text{stat}}] &= \prod_{\vec{x}} \det \left[1 + h_1 W(\vec{x}) \right]^2 \det \left[1 + \bar{h}_1 W^\dagger(\vec{x}) \right]^2 \\ &= \prod_{\vec{x}} \left[1 + h_1 L_{\vec{x}} + h_1^2 L_{\vec{x}}^\dagger + h_1^3 \right]^2 \left[1 + \bar{h}_1 L_{\vec{x}}^\dagger + \bar{h}_1^2 L_{\vec{x}} + \bar{h}_1^3 \right]^2, \end{aligned} \quad (2.8)$$

with the leading order couplings

$$h_1 = (2\kappa e^{a\mu})^{N_\tau}, \quad \bar{h}_1 = (2\kappa e^{-a\mu})^{N_\tau}. \quad (2.9)$$

In order to compute a systematic hopping expansion, we define the kinetic quark determinant

$$\det[Q] \equiv \det[Q_{\text{stat}}] \det[Q_{\text{kin}}], \quad (2.10)$$

$$\det[Q_{\text{kin}}] = [1 - (1 - T)^{-1} (S^+ + S^-)] \equiv \det[1 - P - M] = \exp[\text{tr} \ln(1 - P - M)]. \quad (2.11)$$

The static propagator $(1 - T)^{-1}$ is also known exactly. It contains summation of all temporal windings to produce the basic building blocks of the effective action, for details see [17],

$$W_{n,m}(\vec{x}) = \text{tr} \frac{(h_1 W(\vec{x}))^m}{(1 + h_1 W(\vec{x}))^n}. \quad (2.12)$$

We have calculated the effective action through order $\kappa^8 u^5$ in the low temperature limit, i.e. the leading power of N_τ . However, because of its length we will give the result only in a compact, graphical representation. We symbolise factors of $W_{n,m}(\vec{x})$ by vertices, where n is the number of bonds entering a vertex, and m is the number indicated on the node. Furthermore, vertices which are connected by one or more bonds are nearest neighbours on the lattice.

$$\begin{aligned} S_{\text{eff}} = & h_2 N_f \sum_{\text{dof}} \begin{array}{c} \textcircled{1} \\ | \\ \textcircled{1} \end{array} - h_2^2 N_f \sum_{\text{dof}} \begin{array}{c} \textcircled{1} \\ / \quad \backslash \\ \textcircled{1} \quad \textcircled{1} \end{array} - h_2^2 N_f^2 \sum_{\text{dof}} \begin{array}{c} \textcircled{1} \\ | \\ \textcircled{1} \\ | \\ \textcircled{1} \end{array} + h_2^3 N_f \sum_{\text{dof}} \begin{array}{c} \textcircled{1} \\ / \quad \backslash \\ \textcircled{1} \quad \textcircled{1} \\ / \quad \backslash \\ \textcircled{1} \quad \textcircled{1} \end{array} \\ & + \frac{1}{3} h_2^3 N_f \sum_{\text{dof}} \left(\begin{array}{c} \textcircled{1} \\ / \quad \backslash \\ \textcircled{1} \quad \textcircled{1} \\ / \quad \backslash \\ \textcircled{1} \quad \textcircled{2} \end{array} - \begin{array}{c} \textcircled{1} \\ / \quad \backslash \\ \textcircled{1} \quad \textcircled{2} \\ / \quad \backslash \\ \textcircled{1} \quad \textcircled{1} \end{array} \right) + 2 h_2^3 N_f^2 \sum_{\text{dof}} \left(\begin{array}{c} \textcircled{1} \\ / \quad \backslash \\ \textcircled{1} \quad \textcircled{1} \\ / \quad \backslash \\ \textcircled{1} \quad \textcircled{2} \end{array} - \begin{array}{c} \textcircled{2} \\ / \quad \backslash \\ \textcircled{1} \quad \textcircled{1} \\ / \quad \backslash \\ \textcircled{1} \quad \textcircled{1} \end{array} \right) \\ & + \frac{1}{6} h_2^3 N_f \sum_{\text{dof}} \left(\begin{array}{c} \textcircled{1} \\ | \\ \textcircled{1} \\ | \\ \textcircled{2} \end{array} - \begin{array}{c} \textcircled{2} \\ | \\ \textcircled{2} \end{array} \right) - \frac{4}{3} h_2^3 N_f^3 \sum_{\text{dof}} \begin{array}{c} \textcircled{1} \\ | \\ \textcircled{2} \end{array} - h_2^4 N_f \sum_{\text{dof}} \begin{array}{c} \textcircled{1} \\ / \quad \backslash \\ \textcircled{1} \quad \textcircled{1} \\ / \quad \backslash \\ \textcircled{1} \quad \textcircled{1} \end{array} \\ & - \frac{1}{12} h_2^4 N_f \sum_{\text{dof}} \left(\begin{array}{c} \textcircled{1} \quad \textcircled{1} \\ / \quad \backslash \\ \textcircled{1} \quad \textcircled{1} \\ / \quad \backslash \\ \textcircled{1} \quad \textcircled{1} \end{array} - 2 \begin{array}{c} \textcircled{1} \quad \textcircled{1} \\ / \quad \backslash \\ \textcircled{1} \quad \textcircled{2} \\ / \quad \backslash \\ \textcircled{1} \quad \textcircled{1} \end{array} + \begin{array}{c} \textcircled{1} \quad \textcircled{1} \\ / \quad \backslash \\ \textcircled{1} \quad \textcircled{3} \\ / \quad \backslash \\ \textcircled{1} \quad \textcircled{1} \end{array} \right) - h_2^4 N_f \sum_{\text{dof}} \left(\begin{array}{c} \textcircled{1} \quad \textcircled{1} \\ / \quad \backslash \\ \textcircled{1} \quad \textcircled{1} \quad \textcircled{1} \\ / \quad \backslash \\ \textcircled{1} \quad \textcircled{2} \quad \textcircled{1} \end{array} - \begin{array}{c} \textcircled{1} \quad \textcircled{1} \\ / \quad \backslash \\ \textcircled{1} \quad \textcircled{2} \quad \textcircled{1} \end{array} \right) \\ & - h_2^4 N_f^2 \sum_{\text{dof}} \left(\begin{array}{c} \textcircled{1} \\ | \\ \textcircled{1} \\ | \\ \textcircled{1} \end{array} - 4 \begin{array}{c} \textcircled{1} \\ / \quad \backslash \\ \textcircled{1} \quad \textcircled{2} \\ / \quad \backslash \\ \textcircled{1} \quad \textcircled{1} \end{array} + \begin{array}{c} \textcircled{1} \\ / \quad \backslash \\ \textcircled{1} \quad \textcircled{3} \\ / \quad \backslash \\ \textcircled{1} \quad \textcircled{1} \end{array} \right) - h_2^4 N_f^2 \sum_{\text{dof}} \begin{array}{c} \textcircled{1} \quad \textcircled{1} \\ / \quad \backslash \\ \textcircled{1} \quad \textcircled{1} \end{array} \\ & - 2 h_2^4 N_f^2 \sum_{\text{dof}} \left(\begin{array}{c} \textcircled{1} \quad \textcircled{1} \\ / \quad \backslash \\ \textcircled{1} \quad \textcircled{1} \end{array} - \begin{array}{c} \textcircled{2} \quad \textcircled{1} \\ / \quad \backslash \\ \textcircled{1} \quad \textcircled{1} \end{array} \right) - h_2^4 N_f^2 \sum_{\text{dof}} \left(\begin{array}{c} \textcircled{1} \quad \textcircled{1} \\ / \quad \backslash \\ \textcircled{1} \quad \textcircled{1} \end{array} - 2 \begin{array}{c} \textcircled{1} \quad \textcircled{1} \\ / \quad \backslash \\ \textcircled{1} \quad \textcircled{2} \end{array} + \begin{array}{c} \textcircled{2} \quad \textcircled{1} \\ / \quad \backslash \\ \textcircled{1} \quad \textcircled{2} \end{array} \right) \\ & - \frac{1}{3} h_2^4 N_f \sum_{\text{dof}} \left(\begin{array}{c} \textcircled{1} \\ / \quad \backslash \\ \textcircled{1} \quad \textcircled{1} \end{array} - 2 \begin{array}{c} \textcircled{2} \\ / \quad \backslash \\ \textcircled{1} \quad \textcircled{1} \end{array} + 2 \begin{array}{c} \textcircled{2} \\ / \quad \backslash \\ \textcircled{2} \quad \textcircled{1} \end{array} - \begin{array}{c} \textcircled{3} \\ / \quad \backslash \\ \textcircled{2} \quad \textcircled{1} \end{array} \right) \\ & + \frac{4}{3} h_2^4 N_f^3 \sum_{\text{dof}} \left(\begin{array}{c} \textcircled{1} \\ / \quad \backslash \\ \textcircled{2} \quad \textcircled{1} \end{array} - 2 \begin{array}{c} \textcircled{2} \\ / \quad \backslash \\ \textcircled{2} \quad \textcircled{1} \end{array} + 2 \begin{array}{c} \textcircled{2} \\ / \quad \backslash \\ \textcircled{1} \quad \textcircled{1} \end{array} - \begin{array}{c} \textcircled{3} \\ / \quad \backslash \\ \textcircled{1} \quad \textcircled{1} \end{array} \right) \\ & - \left(\frac{1}{12} N_f + \frac{2}{3} N_f^3 \right) h_2^4 \sum_{\text{dof}} \left(\begin{array}{c} \textcircled{1} \\ / \quad \backslash \\ \textcircled{1} \quad \textcircled{1} \end{array} - 4 \begin{array}{c} \textcircled{2} \\ / \quad \backslash \\ \textcircled{1} \quad \textcircled{1} \end{array} + \begin{array}{c} \textcircled{3} \\ / \quad \backslash \\ \textcircled{1} \quad \textcircled{1} \end{array} \right) - \frac{2}{3} h_2^4 N_f^4 \sum_{\text{dof}} \left(\begin{array}{c} \textcircled{1} \\ | \\ \textcircled{3} \end{array} + 2 \begin{array}{c} \textcircled{2} \\ | \\ \textcircled{2} \end{array} \right) \\ & - \frac{1}{12} h_2^4 N_f^2 \sum_{\text{dof}} \left(\begin{array}{c} \textcircled{1} \\ | \\ \textcircled{1} \end{array} + 12 \begin{array}{c} \textcircled{2} \\ | \\ \textcircled{2} \end{array} + \begin{array}{c} \textcircled{3} \\ | \\ \textcircled{3} \end{array} \right) + \frac{2}{3} h_2^4 N_f^2 \sum_{\text{dof}} \left(\begin{array}{c} \textcircled{1} \\ | \\ \textcircled{2} \end{array} + \begin{array}{c} \textcircled{2} \\ | \\ \textcircled{3} \end{array} \right) + \mathcal{O}(\kappa^{10}) \quad (2.13) \end{aligned}$$

The effective couplings to this order are

$$h_1 = e^{N_\tau(a\mu + \log(2\kappa))} e^{6N_\tau \kappa^2 u \left(\frac{1}{1-u} + 4u^4 - 12\kappa^2 + 9\kappa^2 u + 4\kappa^2 u^2 - 4\kappa^4 \right)}, \quad (2.14)$$

$$h_2 = \frac{\kappa^2 N_\tau}{N_c} \left[1 + \frac{2u}{1-u} + 8u^5 \right]. \quad (2.15)$$

The sign problem of this effective theory is weak and it can be simulated either by complex Langevin without any convergence or runaway problems, or even by standard Metropolis using reweighting. For details and tests of the simulation algorithm see [17].

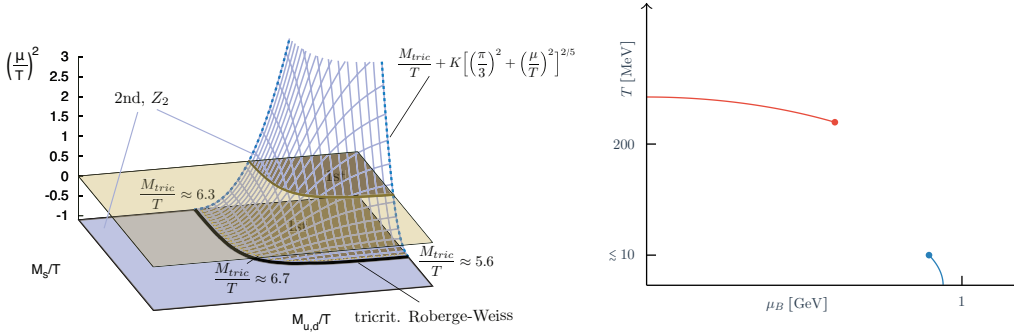


Figure 1: Left: The deconfinement critical surface with heavy quarks for real and imaginary chemical potential. From [15]. Right: The qualitative phase diagram for QCD with heavy quarks. The location of the lines and critical endpoints depends on N_f and the quark mass.

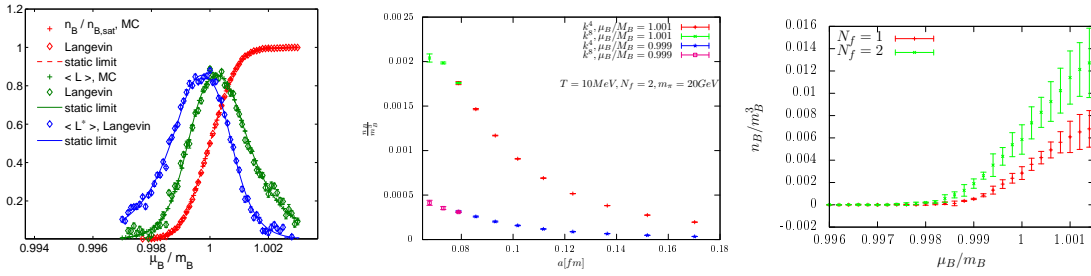


Figure 2: Left: Baryon density, Polyakov loop and conjugate Polyakov loop obtained from Monte Carlo $N_s = 3$, complex Langevin ($N_s = 6$) and the static strong coupling limit, respectively. From [16]. Middle: Continuum extrapolation for two densities. Right: Baryon density in the continuum. From [17].

3. The QCD phase diagram for heavy quarks

The effective theory has been used to study the QCD phase diagram for QCD with heavy quarks. In the static limit, the finite temperature deconfinement transition is of first order, corresponding to the spontaneous breaking of centre symmetry. With dynamical quarks, the fermion determinant breaks the symmetry explicitly and the transition weakens until it changes to a crossover at a critical quark mass. Similarly, real chemical potential weakens the transition. This behaviour is reflected in the heavy mass corner of the Columbia plot. Fig. 1 (left) shows the deconfinement critical surface separating the first order from the crossover region as calculated with a κ^2 -action but full N_τ -dependence in [15].

The cold and dense regime was considered in [16, 17]. Fig. 2 (left) shows results at a fixed lattice spacing. We set the scale using the r_0 parameter and compute the corresponding pion mass from strong coupling formulae [17]. To keep our truncated series in full control, we choose $\beta = 5.7$, $\kappa = 0.0000887$, $N_\tau = 116$ corresponding to $m_\pi = 20$ GeV, $T = 10$ MeV, $a = 0.17$ fm. The silver blaze property as well as lattice saturation are clearly observed. Note that the Polyakov loop as well as its conjugate get screened in the presence of a baryonic medium, and hence rise. The ensuing decrease is due to the artefact of lattice saturation which forces all $Z(3)$ states to be occupied. Note that this decrease happens before saturation near the point of half filling. There is an approximate particle anti-particle symmetry about this point and one expects artefacts to be

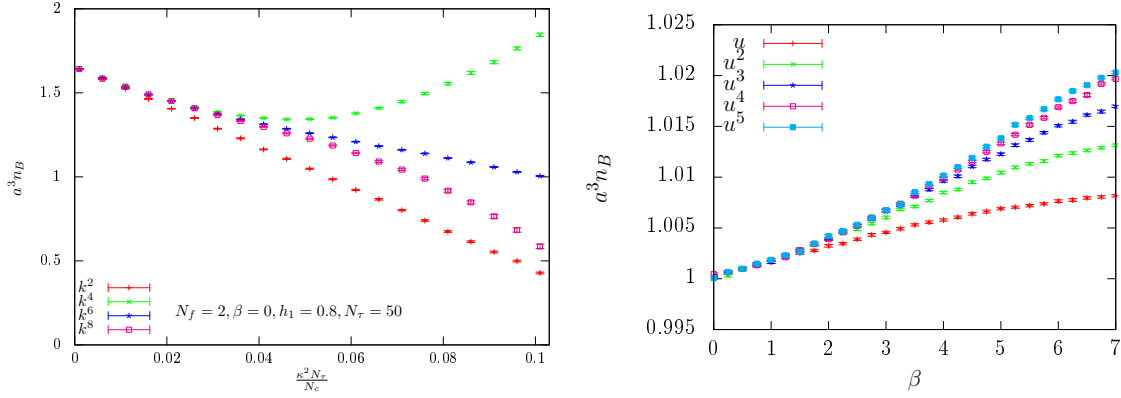


Figure 3: Left: Convergence of the baryon density as a function of $h_2 = \frac{\kappa^2 N_c}{N_c}$, computed with effective actions of different orders in the hopping expansion. Right: Convergence in u .

dominant [18]. Fig. 2 (right) shows the continuum extrapolated results for the baryon density as a function of chemical potential, each point being extrapolated from results for 4-7 lattice spacings [17]. We observe the silver blaze property followed by the onset of nuclear matter, which is steeper for $N_f = 2$ than for $N_f = 1$ as expected. Note that the onset transition happens at $\mu_c \lesssim m_B$, due to the binding energy between the nucleons. Note also that the onset transition here is a smooth crossover, in contrast to the first-order phase transition for physical QCD in nature. This is due to the fact that the binding energy decreases with growing quark mass and for the heavy quarks studied here is smaller than the temperature realized in the plot. It was confirmed in [17] that the first-order behaviour indeed results for sufficiently large hopping parameters/small quark masses, but in that mass range the effective theory is not yet converging and terms of higher order in κ are necessary to quantitatively reproduce QCD.

4. Systematics of the effective theory to order κ^8

An important question is for which parameter regions the effective theory is valid. Since both the character as well as the hopping expansion provide convergent series within their radius of convergence, we are able to self-consistently check this by comparing physical observables at different orders of the effective action. Here we are interested in the cold and dense region around the onset of nuclear matter and our observable of choice is the baryon number. Fig. 3 (left) tests the hopping expansion in the strong coupling limit by comparing results obtained with effective actions of increasing order in κ . One observes clearly how adjacent orders stay together for larger values of the coupling h_2 as the order is increased, thus extending the range where our effective action is reliable. Fig. 3 (right) shows the same exercise for the largest $h_2 \sim 0.1$ considered here, this time increasing the orders of the character expansion. We observe good convergence up to $\beta \sim 7$, which is a sufficiently weak coupling to allow for continuum extrapolations. It is interesting to note that the convergence properties are not determined by the size of the expansion parameters alone. Even though the $u(\beta)$ -values far exceed the κ -values employed in the figures, convergence in $u(\beta)$ appears to be faster.

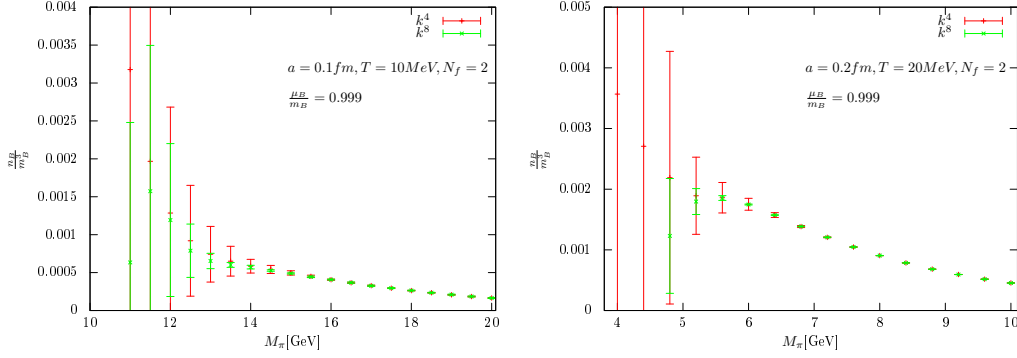


Figure 4: Baryon number density as a function of pion mass.

The gain in convergence region can be exploited in two ways. Firstly, at fixed temperature and quark masses it allows for the use of finer lattices, which can be employed in a continuum extrapolation. Fig. 2 (middle) shows results from our previous simulations obtained with the κ^4 -action as well as new ones with the κ^8 -action at two values of $\mu > \mu_c$. The baryon density just about reaches the domain with leading cut-off effects linear in a , as is expected for Wilson fermions. The break-off from this behaviour for finer lattices is due to truncation errors and indicates the limit of validity of the effective action. The new data generated with the κ^8 -action indeed smoothly extends the linear section towards the continuum limit. We conclude that our hopping expansion is systematic and controlled, with additional orders in the action allowing for simulations on finer lattices. For sufficiently heavy masses a continuum extrapolation appears possible.

A second way to benefit from the additional orders in the hopping expansion is to keep the lattice spacing fixed and study smaller masses. This is shown in Fig. 4 for two different lattice spacings. The error bars in these plots are systematic and give the difference between results obtained by the action to the highest two orders in the hopping expansion. Growing error bars thus indicate the loss of good convergence. As expected, increasing orders allow for smaller quark masses, and so do coarser lattices. However, the gain in mass range per additional order in the hopping expansion is too small to envisage an extension to the physical quark masses of QCD at the present stage.

5. Analytic evaluation of the effective theory

So far we have used Monte-Carlo and Complex Langevin simulations to simulate the effective theory on a 3d lattice and numerically calculate the remaining integral over Polyakov loops. However, restricted to some finite order in the expansion parameters κ and $u(\beta)$, these integrals can also be carried out analytically. In particular, since the effective couplings are small and correspond to power series in the original couplings, a perturbative evaluation should have good convergence behaviour, as noted before [9, 17]. In order to get the correct thermodynamic limit we now employ a linked cluster expansion, and thus calculate the free energy directly rather than going through the partition function. A review of the standard linked cluster expansion can be found in [19]. One should note however that the standard linked cluster expansion tailored to spin models deals with nearest neighbour interactions. Our action on the other hand contains n -point interactions at all dis-

tances and with all possible geometries. It can then be mapped into a spin model, whose partition function thus takes the more generalised form

$$\mathcal{Z} = \int \prod_{x,i} d\phi_i(x) \exp \left\{ -S_0[\phi_i] - \frac{1}{2!} \sum_{x,y} v_{ij}(x,y) \phi_i(x) \phi_j(x) - \frac{1}{3!} \sum_{x,y,z} u_{ijk}(x,y,z) \phi_i(x) \phi_j(y) \phi_k(z) + \dots \right\}. \quad (5.1)$$

In our case the effective theory is fully encoded in the coupling constants $v_{ij}(x,y), u_{ijk}(x,y,z), \dots$, which themselves are series in the expansion parameters. The free energy can hence be rewritten as:

$$\mathcal{W}[v, u, \dots] = \left[\exp \left(\frac{1}{2!} \sum_{x,y} \sum_{i,j} v_{ij}(x,y) \frac{\delta}{\delta \tilde{v}_{ij}(x,y)} \right) \exp \left(\frac{1}{3!} \sum_{x,y,z} \sum_{i,j,k} u_{ijk}(x,y,z) \frac{\delta}{\delta \tilde{u}_{ijk}(x,y,z)} \right) \dots \right] \mathcal{W}[\tilde{v}, \tilde{u}, \dots] \Big|_{\substack{\tilde{v}=0 \\ \tilde{u}=0 \\ \dots}}, \quad (5.2)$$

and with the expressions for the couplings at hand, the 3d theory can be evaluated analytically in a systematic, well defined way by carrying out the higher order derivatives and summing over the set of topologically invariant terms. Although this approach is valid, it lacks the elegance of the graphical techniques of the linked cluster expansion. However, because the all of the terms given in Eq. (2.13) can be embedded on a square lattice, one can use another embedding scheme to simplify the calculations. This scheme will be introduced next.

6. Graphical methods

The linked cluster expansion graphs constitute all contributions to the free energy in the thermodynamic limit up to a certain order. Therefore by embedding the terms from the effective action onto all connected skeleton graphs from the linked cluster expansion with two-point interactions, we can calculate the free energy of the effective theory. This procedure is most easily demonstrated with an example:

Consider for now an effective theory consisting of two terms, a nearest neighbour term, and a "wedge"

$$S = a \sum_{\text{dof}} \text{---} + b \sum_{\text{dof}} \text{---} \cdot \quad (6.1)$$

To calculate the free energy, we can embed these terms onto the linked cluster graphs, calculating symmetry factors and lattice embeddings for every embedding on every graph. For example embedding onto the fourth order graph

$$g_8 = \text{---} \cdot, \quad \text{symmetry: } 4 \quad (6.2)$$

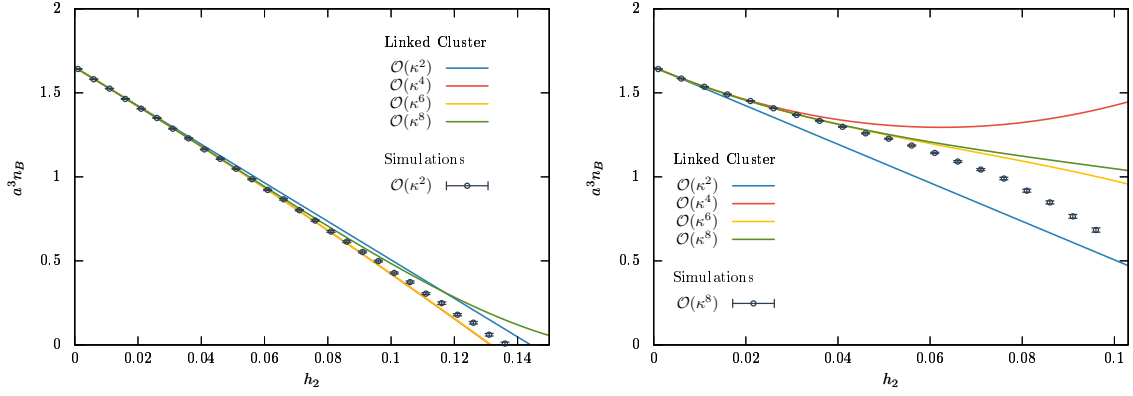


Figure 5: Linked cluster expansion of the κ^2 (left) and κ^8 (right) actions for $\beta = 0$ and $h_1 = 0.8$.

we get the following contribution to \mathcal{W} :

$$\mathcal{W}_{gs} = \frac{a^4 \Lambda}{4} \text{diagram} + a^2 b \Lambda \text{diagram} + \frac{a^2 b \Lambda}{2} \text{diagram} + \frac{b^2 \Lambda}{2} \text{diagram}. \quad (6.3)$$

The denominators give the overall symmetry factor of the embedding and Λ is the lattice embedding of the graph itself. For d dimensional square lattices it is $\Lambda = (2d)^3$. After the embeddings we are left with overlapping nodes at individual lattice points which gives integrals on the form

$$\int dW \det [Q_{\text{stat}}]^{2N_f} W_{n_1, m_1}^{k_1} \dots W_{n_N, m_N}^{k_N}, \quad (6.4)$$

which are analytically calculable for $\sum_i n_i k_i \leq 2N_f$ using for example Polyakov loop integral lookup tables. This means that for a system with 2 degenerate quark flavours we can carry out the calculation up to order κ^8 . The full result for the free energy is too lengthy to be included here, and will be published elsewhere in the near future.

7. Comparison with numerics

With an analytic expression for the free energy at hand, various bulk thermodynamic quantities can be calculated and the results compared to those obtained with numerics. It should be stressed that the analytical results emerged from a two stage, first the effective action is calculated to a fixed order. Second, the expanded action is used to compute e.g. the free energy to a specific order. This implies that we have for example a $\mathcal{O}(\kappa^8)$ linked cluster expansion for the $\mathcal{O}(\kappa^2)$ action, which we expect to reproduce the $\mathcal{O}(\kappa^2)$ numerical results. A comparison between the various orders of the linked cluster expansion is presented in Fig. 5. Expanding the κ^2 action is shown to the left, while the κ^8 action is used in the right plot. From the figure one can see that the κ^2 action converges much quicker than the κ^8 action. This is only natural as the cluster expansion to order κ^4 only contains effective action terms to the same order, and the expansion thus have to "catch up" with the order at hand.

A linked cluster expansion is done for a fixed lattice spacing. By applying the same procedure to different lattices it is also possible to carry out continuum extrapolations. In Fig. 6 (left) it

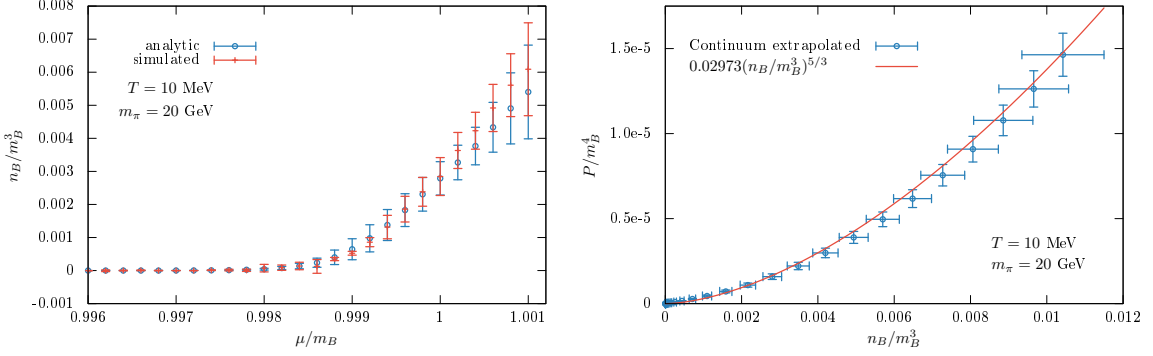


Figure 6: Continuum extrapolated results from the analytic calculation. Left: Baryon density as a function of baryon chemical potential, compare to Fig. 2. Right: The equation of state in the cold and dense regime with a fitted curve.

is demonstrated that this gives remarkably similar results to the numerical ones. In both cases error bars include a systematic error, measured as the difference between the two highest order effective actions. Fig. 6 (right) shows a continuum extrapolated equation of state for the dense nuclear matter. It is interesting to note that when the curve is fitted to a power law, the exponent suggests that heavy dense matter behaves as a non-relativistic free gas of fermions. The origin of this behaviour will be the subject of further study and we believe that analytical equations will be helpful in this endeavour as one can turn on and off the interconnected degrees of freedom to obtain insight into the underlying processes at work.

8. Chain resummation

So far we have managed to reproduce most of the simulated results with analytical calculations. In this section we will present a resummation scheme for the analytic approach which even extends its reach beyond that of the numerical methods. First let us demonstrate the pattern with a small example before moving on to the full resummation. Consider for now the following four terms from Eq. (2.13),

$$h_2 N_f \sum_{\text{dof}} \begin{array}{c} \textcircled{1} \\ | \\ \textcircled{1} \end{array}, -h_2^2 N_f \sum_{\text{dof}} \begin{array}{c} \textcircled{1} \\ / \quad \backslash \\ \textcircled{1} \quad \textcircled{1} \end{array}, h_2^3 N_f \sum_{\text{dof}} \begin{array}{c} \textcircled{1} \quad \textcircled{1} \\ / \quad \backslash \\ \textcircled{1} \quad \textcircled{1} \end{array}, -h_2^4 N_f \sum_{\text{dof}} \begin{array}{c} \textcircled{1} \quad \textcircled{1} \\ / \quad \backslash \\ \textcircled{1} \quad \textcircled{1} \end{array}. \quad (8.1)$$

It is easy to see a common pattern appearing from these terms. Each term extends the length of the chain by one node while maintaining a common prefactor. Looking at the equations we see that every link in the chain adds a factor $h_2 W_{2,1}$ to the term, along with the necessary spatial geometry. One can check with the terms up to order κ^8 in Eq. (2.13) that this holds not only for the simple chain shown above, but for all terms in the action with a singly connected node, meaning nodes that correspond to a factor of $W_{1,1}$. The "chain" resummation scheme thus corresponds to the substitution

$$W_{1,1}(x) \rightarrow W_{1,1}(x) \sum_{n=0}^{\infty} \mathcal{G}(\{x_n\}) \prod_{i=1}^n (-h_2) W_{2,1}(x_i), \quad (8.2)$$

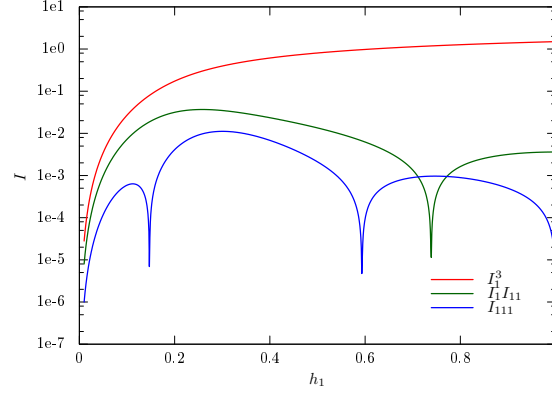


Figure 7: Value of the integrated nodes where the red curve comes from three separate nodes, the green curve from the case where two of the three nodes overlap and finally the blue curve from the case where all three nodes overlap.

where $\mathcal{G}(\{x_n\})$ contains the geometry of the chain. We will not go into more detail about the correctness of the chain resummation here as it is quite involved. A more satisfactory argument based on the specifics of the effective 3d theory will be given in a separate publication.

While we now have a resummation to all orders in κ for every order in the effective theory, evaluating the final gauge integral is still impossible. This is because we need to sum over all geometries for all the terms in the resummation, which is inaccessible. To proceed, an additional constraint must be introduced, namely that only embeddings with the same basic geometry as the chain itself is included. This implies that all nodes of the chain will be at separate lattice points, and an $n + 1$ long chain will result in the following integral:

$$\left((2d)h_2 \int dW \det [Q_{\text{stat}}]^{2N_f} W_{2,1} \right)^n (2d)h_2 \int dW \det [Q_{\text{stat}}]^{2N_f} W_{1,1} \equiv (2dh_2)^{n+1} I_{11} I_{21}^n. \quad (8.3)$$

and thus the full chain will give

$$(2d)h_2 I_{11} \sum_{n=0}^{\infty} (-(2d)h_2)^n I_{2,1}^n = \frac{(2d)h_2 I_{11}}{1 + (2d)h_2 I_{21}}. \quad (8.4)$$

Carrying out this resummation also introduces a small error. This arises because the embedding factor of $(2d)$ is too large, and the linked cluster expansion relies on cancellations from other same order graphs to correct this. These would be graphs that overlap with itself as it spans the lattice. One could replace the embedding factor with a more natural one from e.g. studies of the self-avoiding walk. For a 3d square lattice the factor would be somewhere between 4 and 5. However, in Fig. 7 one can clearly see that the contributions from self-overlapping terms are subleading, especially as we increase the baryon chemical potential.

9. Resummed results

With the improved analytical results at hand we redo the convergence plot. In Fig. 8 (left) the effects of the resummation are clearly visible, more than doubling the convergence region in h_2 .

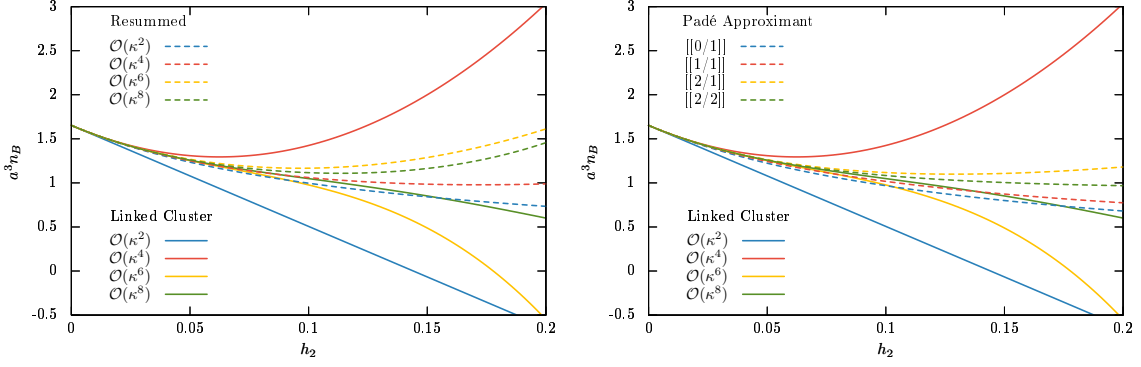


Figure 8: Convergence of the analytically improved 3d theory results. Left: Using the resummation scheme introduced in Section 8. Right: Using the near diagonal Padé approximants.

On the right of the same figure we have also provided the result of carrying out a Padé approximation in h_2 , choosing the close to diagonal ones. It is not surprising that the Padé approximation gives similar improvements, although slightly superior. Both correspond to resummations giving rational expressions. The Padé is not restricted to a particular class of diagrams and might therefore predict more of the higher order behaviour. Nonetheless, the similarity between the two results is reassuring as to the validity of the chain resummation, which originates from the effective theory itself.

Finally, we use this improved convergence behaviour to study another physics observable. In Fig. 9 we plot the binding energy per nucleon, defined by the energy density minus the mass density in the zero temperature limit,

$$\varepsilon \equiv \frac{e - n_B m_B}{n_B m_B}. \quad (9.1)$$

This is an important quantity that characterises nuclear matter. In previous work we have shown numerically and to leading order in the hopping expansion, that it displays the silver blaze property until the onset transition, where it becomes negative [17]. We can now extend this study to slightly larger densities. Fig. 8 shows the binding energy extracted from both the resummation scheme as well as the Padé approximants to the partition function at various orders. While quantitative convergence breaks down shortly after the onset transition near $3\mu \sim m_B$, we obtain a new qualitative result: in higher orders we see the binding energy becoming positive again with growing chemical potential, as is expected from nuclear physics. A minimum characterising nuclear density appears, which however is not yet settled quantitatively at the available orders.

10. Conclusion

In a continuation of a long term project, we have derived a 3d effective lattice action for the description of thermodynamics of QCD with heavy quarks through the orders $u^5 \kappa^8$ in a combined character and hopping parameter expansion. The effective action can be simulated by either complex Langevin or, due to the mildness of its sign problem, Metropolis with reweighting. By

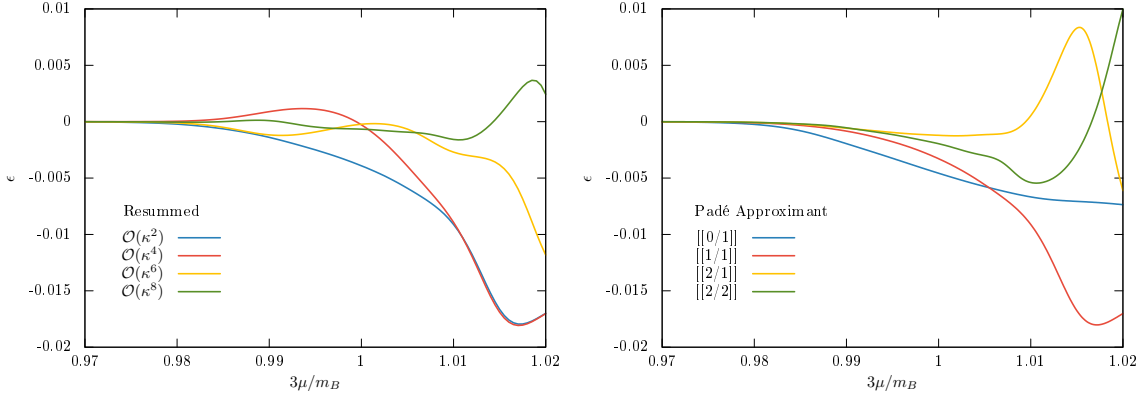


Figure 9: Plots of the binding energy as a function of baryon chemical potential, $\beta = 0$, $\kappa = 0.08$, $N_t = 50$. Left: Using the resummation scheme. Right: Using the Padé approximants.

comparing results for observables obtained with effective actions of neighbouring orders, full control over the convergence properties of the expansion is obtained. The additional orders in the effective action allow for finer lattices and somewhat lighter quark masses, though an extension to the physically interesting mass region is not in reach at present. By generalising linked cluster expansion methods from spin models to our effective lattice theory with long distance and many-point couplings, a fully analytic calculation of thermodynamic functions was achieved that quantitatively agrees with the simulations of the effective theory. Finally, we have devised a resummation scheme that sums up infinite chains of graphs analytically, which in addition includes higher order terms in the effective theory.

Acknowledgments

This project was supported by the German BMBF, No. 06FY7100 as well as by the Helmholtz International Center for FAIR within the LOEWE program of the State of Hesse.

References

- [1] P. de Forcrand, PoS LAT **2009** (2009) 010 [arXiv:1005.0539 [hep-lat]].
- [2] G. Aarts, F. Attanasio, B. Jäger, E. Seiler, D. Sexty and I. O. Stamatescu, arXiv:1412.0847 [hep-lat].
- [3] G. Aarts, F. Attanasio, B. Jäger, E. Seiler, D. Sexty and I. O. Stamatescu, arXiv:1510.09100 [hep-lat].
- [4] P. Scior, D. Scheffler, D. Smith and L. von Smekal, PoS LATTICE **2014** (2015) 173 [arXiv:1412.7089 [hep-lat]].
- [5] P. Scior and L. von Smekal, arXiv:1508.00431 [hep-lat].
- [6] C. Wozar, T. Kaestner, A. Wipf and T. Heinzl, Phys. Rev. D **76** (2007) 085004 [arXiv:0704.2570 [hep-lat]].
- [7] J. Greensite and K. Langfeld, Phys. Rev. D **88** (2013) 074503 [arXiv:1305.0048 [hep-lat]].
- [8] J. Greensite and K. Langfeld, Phys. Rev. D **90** (2014) 014507 [arXiv:1403.5844 [hep-lat]].

- [9] G. Bergner, J. Langelage and O. Philipsen, arXiv:1505.01021 [hep-lat].
- [10] J. Langelage, S. Lottini and O. Philipsen, JHEP **1102** (2011) 057 [Erratum-ibid. **1107** (2011) 014] [arXiv:1010.0951 [hep-lat]].
- [11] J. Langelage, S. Lottini and O. Philipsen, PoS LATTICE **2010** (2010) 196 [arXiv:1011.0095 [hep-lat]].
- [12] J. Langelage and O. Philipsen, JHEP **1001** (2010) 089 [arXiv:0911.2577 [hep-lat]].
- [13] J. Langelage and O. Philipsen, JHEP **1004** (2010) 055 [arXiv:1002.1507 [hep-lat]].
- [14] T. C. Blum, J. E. Hetrick and D. Toussaint, Phys. Rev. Lett. **76** (1996) 1019 [hep-lat/9509002].
- [15] M. Fromm, J. Langelage, S. Lottini and O. Philipsen, JHEP **1201** (2012) 042 [arXiv:1111.4953 [hep-lat]].
- [16] M. Fromm, J. Langelage, S. Lottini, M. Neuman and O. Philipsen, Phys. Rev. Lett. **110** (2013) 122001 [arXiv:1207.3005 [hep-lat]].
- [17] J. Langelage, M. Neuman and O. Philipsen, JHEP **1409** (2014) 131 [arXiv:1403.4162 [hep-lat]].
- [18] T. Rindlisbacher and P. de Forcrand, arXiv:1509.00087 [hep-lat].
- [19] M. Wortis, In *Domb, C., Green, M.S.: Phase Transitions and Critical Phenomena, Vol.3*, 113-180